The Journal of the Korean Society of Oceanography
Vol. 31, No. 2, pp. 64-74, June 1996

Numerical Experiments of Ocean Acoustic Tomography in the East Sea of Korea

SANG KYU HAN, JUNG YUL NA AND JAE HAK LEE[1]
Dept. of Earth and Marine Sciences Hanyang University, Ansan, 425-791, KOREA
[1]Physical Oceanography Division, Korea Ocean Research and Development Institute, Ansan, 425-600, KOREA

Numerical experiments of OAT (Ocean Acoustic Tomography) are carried out in the East Sea of Korea where the canonical ocean has been perturbed by a mesoscale warm eddy and a thermal front. In order to estimate the horizontal and vertical structure of water temperature of the perturbed ocean, the experimental area is divided into 16 cells with 8 pairs of sources and receivers for a horizontal slice and the water column is divided into 8 layers for a vertical slice. The inversely estimated temperature field by using SVD (Singular Value Decomposition) method reveals the eddy and frontal structure clearly. The rms errors of the two horizontal slices are less than 0.4°C and 1.7°C at 400 m and 200 m depths, respectively, while the error in the vertical slice is less than 1.0°C. For better estimation of temperature by OAT method, particularly for the East Sea, a range-dependent ray model should be used to solve the forward problem. At the same time, improvement in computing the refracted ray path between vertical layers is required to obtain more accurate travel time information. The results of the present experiment give rise to a possibility of application of OAT in remote sensing of the ocean thermal structure.

INTRODUCTION

Since Munk and Wunsch (1979) proposed the basic principle of Ocean Acoustic Tomography (OAT), it has become one of the most promising approaches to monitor the thermal structure of the ocean interior. The OAT is a remote sensing technique based on the fact that the travel time of sound wave depends on the physical properties of the propagating media. The travel time deviation from a reference state, e. g. the canonical ocean, implies the perturbation in the ocean and can be used to determine the perturbed sound speed fields.

As a technology of ocean survey, the OAT requires three separate procedures: a forward problem, an acoustic experiment and an inverse problem. The forward problem is to establish the reference travel time of each eigenray between a fixed source and a receiver assuming that properties of a inhomogeneous media are known. It is required that the variation of acoustic travel times must satisfy the necessary conditions of ray path stability, identification and resolution (Spiesberger *et al.*, 1980). The acoustic experiment is to measure the travel time perturbations due to oceanic fluctuations, and the inverse problem is to obtain the sound speed variations from the difference between observed travel time and predicted (canonical ocean) one.

The OAT in oceanic survey gives several advantages for studying temporal and spatial fluctuations of oceanic structure (Worcester *et al.*, 1991). The OAT experiments have shown that the ocean mesoscale structure is highly effective (Cornuelle *et al.*, 1985) and a large-scale oceanic change is detected (Munk and Forbes, 1989). Also a long range reciprocal transmission can be inverted to obtain ocean currents (Howe *et al.*, 1987) and performed to study the fluctuations of the internal wave and internal tide (Lynch *et al.*, 1996). Recently, a real-time OAT system (moving ship OAT etc.) which combines the OAT with satellite-based time keeping and

satellite telemetry (Lynch *et al.*, 1992) has been developed. Detailed literature may be found in Munk *et al.* (1995).

For the East Sea (Japan Sea), Russia and Japan scientists carried out preliminary acoustic tomography study. Akulichev and Solovyov (1993) proposed possible locations of the acoustic source and receiver system with 700~800 km distance. Kaneko *et al.* (1994) designed an acoustic tomography system which can monitor the East Sea in eddy resolving scale through the computer experiments.

Although the use of an OAT for ocean survey is quite active now, Korean oceanographers just began expressing their interests in it. Recently, to develope OAT in the East Sea, a series of studies has been carried out. Paeng (1993) established a canonicalocean from long-term temperature observation and salinity data in the southwestern part of the East Sea, and calculated the acoustic travel time and ray path for the canonical ocean by using a range-independent acoustic propagation model. Han and Na (1994) and Na and Han (1994) tested a forward problem to simulate the received signals with generated random noise by using a range-dependent acoustic model. The results generally satisfied the necessary conditions of OAT.

As a next step, we perform a feasibility study of OAT in the East Sea focusing on the inverse problem. Acoustic travel times in the canonical ocean with an ideal warm eddy or a polar front are computed by the method of ray theory in a range-dependent medium. Then, ocean structures in the horizontal and vertical slices are estimated from the acoustic travel time differences by inverse calculations. In section 2, we describe formulations of OAT. Inverse calculations and results are demonstrated in section 3 and a summary and discussions are presented in section 4.

FORMULATIONS

The ray paths and travel times of a sound wave in the ocean depend on the physical properties (temperature, salinity and pressure) of sea water. The acoustic travel time along a ray path in the ocean between a source and a receiver is given by a function of the sound speed and the current velocity along the ray path.

The travel time (τ_0) along a ray path Γ_0 in the canonical ocean, $C_0(z)$, is given by

$$\tau_0 = \int_{\Gamma_0} \frac{ds}{C_0(z)} \quad (1)$$

In the presence of a perturbation, $\delta C(r, z)$, the exact travel time (τ_1) along a new ray path Γ_1 is

$$\tau_1 = \int_{\Gamma_1} \frac{ds}{C_0 + \delta C(r, z)} \quad (2)$$

Observed sound speed fields are divided into reference state and perturbations, $C(r, z) = C_0(z) + \delta C(r, z)$ where $\delta C \ll C_0$. Then, the travel time difference ($\delta\tau$) can be written as

$$\delta\tau = \tau_1 - \tau_0 = \int_{\Gamma_1} \frac{ds}{C_0 + \delta C} - \int_{\Gamma_0} \frac{ds}{C_0} \quad (3)$$

After some algebraic manipulations (Munk et al., 1995), it reduces to

$$\delta\tau = -\int_{\Gamma_0} \frac{\delta C}{C_0^2} ds + \varepsilon \quad (4)$$

where ε represents the small errors due to the approximations used. Dropping ε, equation (4) becomes the basic equation used in OAT.

Generally, the reference travel time is calculated by using equation (1) through computer modelling and the perturbed travel time is obtained by field experiments. However, in this feasibility study, the latter is obtained from equation (2) assuming that $\delta C(r, z)$ is known for the forward problem. The reconstruction techniques to estimate sound speed, temperature, and current velocity from the acoustic travel time data are an application of standard inverse theory which is frequently used in seismology and other area of oceanography (Aki and Richards, 1980; Bennett, 1992).

If one divides the ocean into several cells, equation (4) can be approximated by a corresponding discrete form,

$$\delta\tau_i = -\sum_{j=1}^{J} \frac{R_{ij}\delta C_j}{C_0^2} \quad (i=1, 2, \cdots, I) \tag{5}$$

where i and j represent ith ray path and jth grid, respectively, R_{ij} the path length, and δC_j the unknown sound speed perturbation averaged over the jth grid. For a given region, one can list the unknown δC_j values as elements of a single vector x and take $-R_{ij}/C_0^2$ as entries in the matrix A to rewrite the problem as a linear algebraic system

$$Ax = b, \tag{6}$$

where b has the components given by $\delta\tau_i$ in equation (5). The size of the matrix A depends on the number of cells and ray paths. It is desirable to make the system overdetermined, i.e., the number of ray paths exceeds that of cells, because the criterion used for obtaining an inverse solution is much more reliable in the case of overdetermined system than the underdetermined one.

To obtain inverse solutions for an overdetermined problem, there are various methods based on the least squares estimate such as a linear regression problem. The most powerful one is the method using the Singular Value Decomposition (SVD, Lanczos, 1961; Bennet, 1992), $U^T AV = \Lambda$, where Λ is a diagonal eigenvalues matrix, and U and V are orthogonal matrices. The method of SVD yields useful information for inversion such as the stability of solution to the noise in the vector b. The solution is given by

$$\hat{x} = V\Lambda^{-1} U^T b. \tag{7}$$

From the solution $\hat{x}(=\delta C)$, sound speed fields for the perturbed ocean can be constructed by using $C = C_0 + \delta C$.

NUMERICAL EXPERIMENTS

Data Sets

Acoustic travel time is primarily given by the integral of sound speed along each ray path. The sound speed C (m/s) can be formulated by using a function of temperature T (°C), salinity S (‰), and depth Z (m) as in Clay and Medwin (1977),

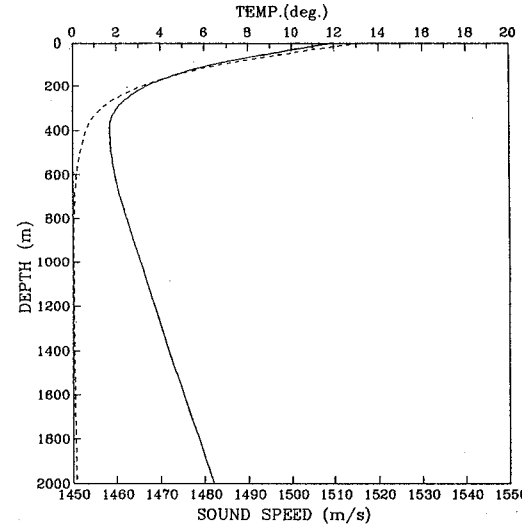

Fig. 1. Sound speed and temperature profile of the canonical ocean in the East Sea obtained from long-term observed data in the study area. Solid and dashed lines correspond to sound speed and temperature.

$$C(T, S, Z) = 1449.2 + 4.6T - 0.055T^2 + 0.00029T^3 + (1.34 - 0.010T)(S-35) + 0.016Z. \tag{8}$$

Because the effects of T on C generally dominate over salinity S especially over the area of interest in present study, the sound speed can be approximated as a function of temperature only. In the following experiment, neglecting the higher-order terms of T and the effect of S, we use the following simplified formula

$$C = 1449.2 + 4.6T + 0.016Z. \tag{9}$$

A rectangular area of 200×200 km with a constant depth, 2500 m, in the southwestern part of the East Sea was chosen as a tomography experiment area. Acoustic travel times and ray paths for the canonical ocean, which represent a mean state of the study area (130~133° E, 35~38° N) determined from the historical temperature and salinity data observed by the FRDA (Fisheries Research and Development Agency, 1986), are used as reference values. The temperatures of the canonical ocean in

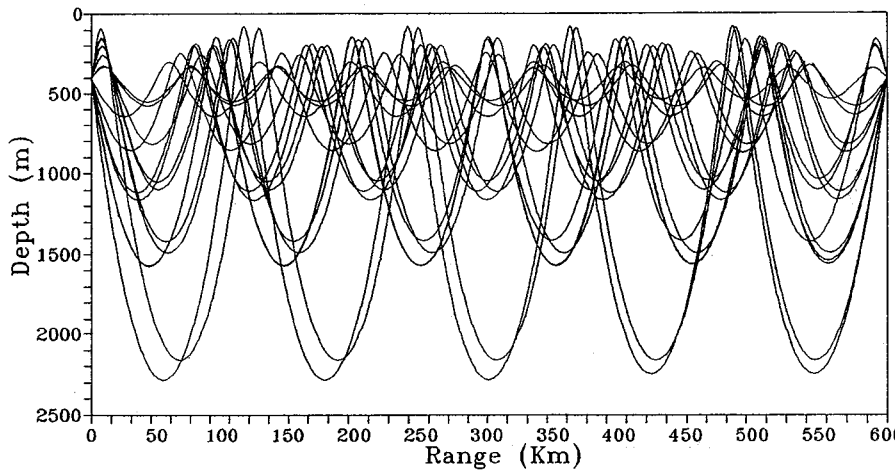

Fig. 2. Eigenray trace of refracted arrivals between a source and a receiver (separated by 200 km) for the canonical ocean. The ray identifiers are summarized in Table 1.

Table 1. Ray identifiers. The identifier presented by n, where positive (negative) rays depart upward (downward) from the source, n^+ and n^- are the total number of upper and lower turning points, θ_S is the departure angle at the source, θ_R is the arrival angle at the receiver, z^+ and z^- are the upper and lower turning depths, respectively, and S is the reference path length

no.	n		θ_S	θ_R	Z^+	Z^-	S
	n^+	n^-	deg	deg	m	m	km
1	4	4	11.16	-11.14	77	2275	201.468
2	-5	4	-10.77	-10.83	86	2159	201.408
3	-5	5	-10.44	10.40	93	2063	201.365
4	5	5	8.50	-8.61	139	1567	200.885
5	-5	4	-8.40	-7.34	141	1544	200.918
6	5	6	8.50	-9.38	139	1566	200.974
7	-6	5	-7.78	8.28	157	1405	200.775
8	5	5	6.53	-6.53	189	1160	200.547
9	-7	6	-6.15	-6.28	200	1095	200.482
10	6	7	6.36	6.68	194	1131	200.573
11	-7	7	-5.93	6.14	206	1058	200.494
12	7	7	4.50	-5.10	247	847	200.279
13	-8	7	-4.10	-4.43	258	795	200.232
14	7	8	4.50	-.86	247	847	200.309
15	8	8	2.98	-2.06	293	665	200.139
16	-9	8	-2.01	-2.43	327	566	200.062
17	-9	9	-1.98	1.17	328	563	200.068

the tomographic site are about 13°C at the surface and about 0.1°C at the depth of sound channel axis (located around 400 m depth). Corresponding sound speed is 1510 and 1458 m/s (Fig. 1), respectively. Acoustic sources and receivers are placed at the depth of sound channel axis along the rim of the study area. Fig. 2 shows the eigenray tracing in the canonical ocean based on the sound speed profile in Fig. 1. The upper most and lower most turning depths are 77 and 2275 m, respectively, in the ray tracing. Source and receiver angles are about $\pm 11°$ (+ is upward and - is downward) and the total number of upper and lower turning is 4. The upper and lower turning depths of the inner most rays are 328 and 563 m, respectively, and departure angle at the source and arrival angle at the receiver are very small. Detailed ray identifiers are summarized in Table 1.

Now, an appropriate temperature structure is added to the canonical ocean and a perturbed acoustic travel time which is regarded as field data for inversion is computed. We consider warm eddy and thermal front as perturbed temperature

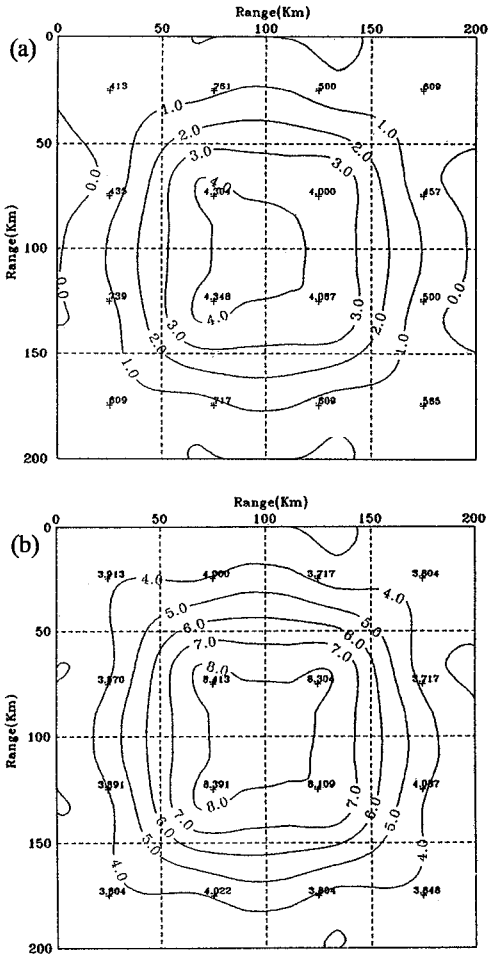

Fig. 3. Distributions of the input temperature in the warm eddy (a) at 400 m depth and (b) 200 m depth. Input values are marked at each grid point. The units is °C.

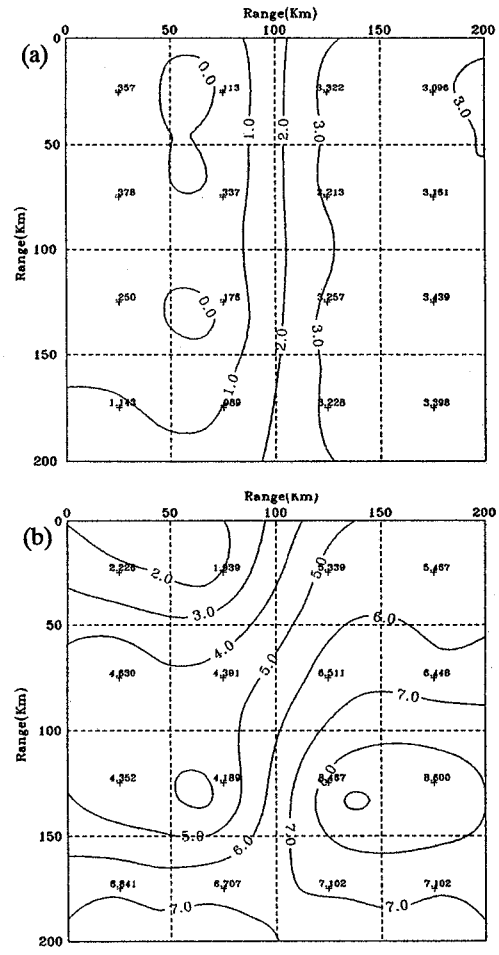

Fig. 4. Distributions of the input temperature in the front (a) at 400 m depth and (b) 200 m depth. Input values are marked at each grid point. The units is °C.

structure. For the warm eddy, horizontal distributions of temperature at 200 and 400 m depths are shown in Fig. 3. The temperatures are higher than 4.0°C in the eddy and about 0.5°C in the outer part at 400 m depth (Fig. 3a). At 200 m depth, temperature increases higher than 8.0°C in the center (Fig. 3b). The temperature differences between canonical ocean and the ocean perturbed by the eddy show negative values at the surface, maximum 5.5°C at 200 m depth, and positive values, 3.0°C below the sound channel axis. In the case of the front, the temperature of colder portion is similar to canonical ocean but the warmer portion shows values higher than 3.0°C at 400 m depth (Fig. 4a). At 200 m depth, the temperatures are higher and the pattern of temperature distribution is different from the one at 400 m depth (Fig. 4b). The temperature deviations from the canonical ocean are complicate showing the maximum 5.0°C at 200 m depth, and less than 2.0°C below the sound channel axis.

In the following numerical experiments, we test two different models: horizontal and vertical slice inversions. The former is focused on the lateral structure of the ocean along the depth of sound channel, the latter determining the vertical profile.

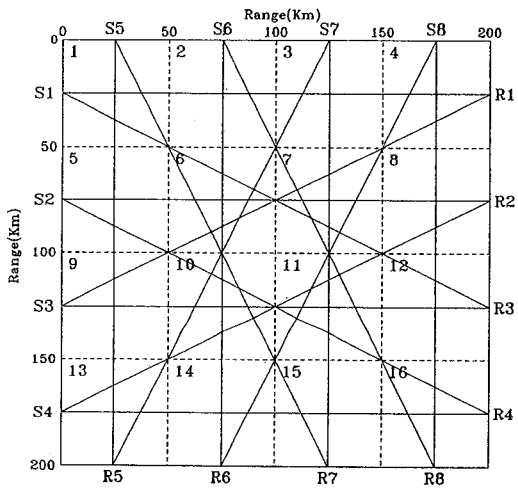

Fig. 5. Plan view of the ocean acoustic tomography experiment with the positions of eight acoustic sources (S1~S8) and eight receivers (R1~R8). The 200 km × 200 km area is divided into 16 grid cells (bounded by dashed lines). The ray paths from sources to receivers are indicated by solid line.

Horizontal Slice Inversion

The experimental area is divided into 16 cells of 50 × 50 km in size. 8 pairs of sources and receivers are placed at the mid point of boundary cells as shown in Fig 5. Because the number of unknowns is 16 in this grid system, more than 16 eigenray information (travel time difference and path length) is needed to make an overdetermined inverse model. The given sources and receivers make 32 route connecting a source and a receiver and we use 16 of them.

The acoustic travel times for 17 rays were computed for all possible routes from the sources to receivers as shown in Table 1. The travel times in the canonical ocean are from 136.5 sec (ray number 1 in Table 1) to 137.2 sec (ray number 17) (Fig. 6). For the perturbed ocean (Fig. 6a), the travel times for the rays passing through the outer part of the warm eddy (ray path S1-R1 or S4-R4) are close to those in the canonical ocean, but those are decreased about 0.5 sec slower when the ray passes the center of the eddy (ray path S2-R2 or S3-R3). In the case of the frontal ocean through which all the rays propagate, the travel times of the acoustic rays

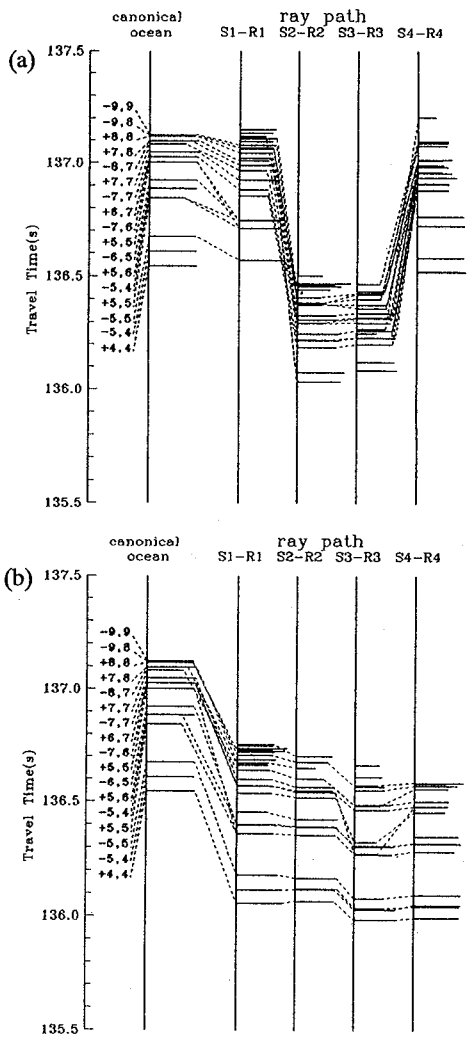

Fig. 6. Comparison of the predicted (canonical ocean) and simulated arrival patterns for (a) the warm eddy and (b) the front. The numbers to the left mean the ray identifiers shown in Table 1. Solid bars in horizontal axis mean the normalized eigenray amplitude. The ray identifiers connected by dashed lines are the ray arrivals actually used. Unexpected arrivals are not connected by dashed line.

are in the range from 136.0 sec to 136.8 sec (Fig. 6b). In any cases, the travel time difference ($\delta\tau_i$) is not larger than 0.6 sec. A single ray path is used in this model: the ray number 15 or 16 defined in Table 1 or the ray number 4 for 400 m and 200 m depths, respectively.

Fig. 7 shows distributions of temperature at 400

m depth determined by inverse method. It reveals the eddy and frontal structure well. Rms (Root-Mean-Square) error is less than 0.4°C as shown in Table 2. The temperature differences between the input data and inversion results show negative values at the central part of the eddy, but the positive at the outer part (Table 2a). For the frontal area, they are positive at the upper left corner and negative at the right one (Table 2b). This implies that the inversion may not recover input data when the structure is extremely perturbed.

While the results at 400 m depth are very encouraging, those at 200 m depth are not. The error of the inversion results at 200 m depth is larger than

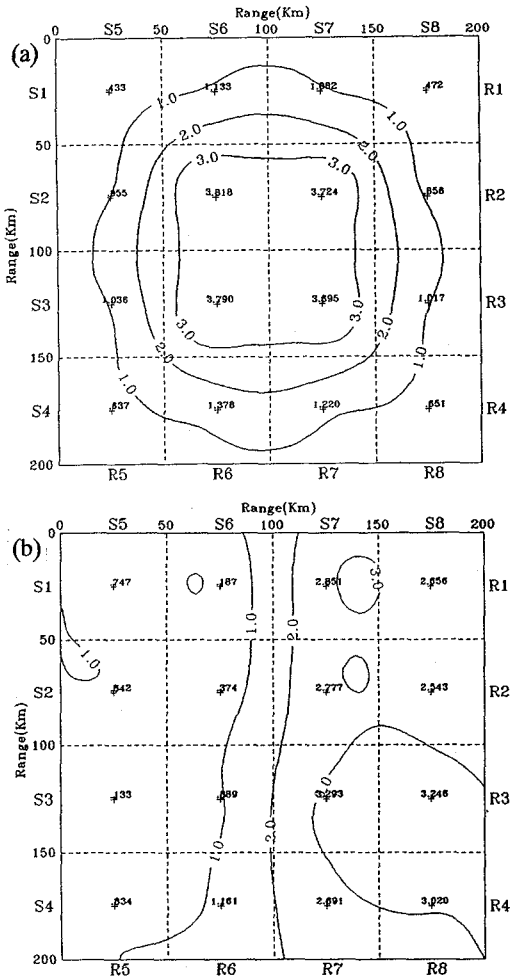

Fig. 7. Distribution of temperature estimated from the results of horizontal slice inversion for (a) the warm eddy and (b) the front at 400 m depth. The units is °C.

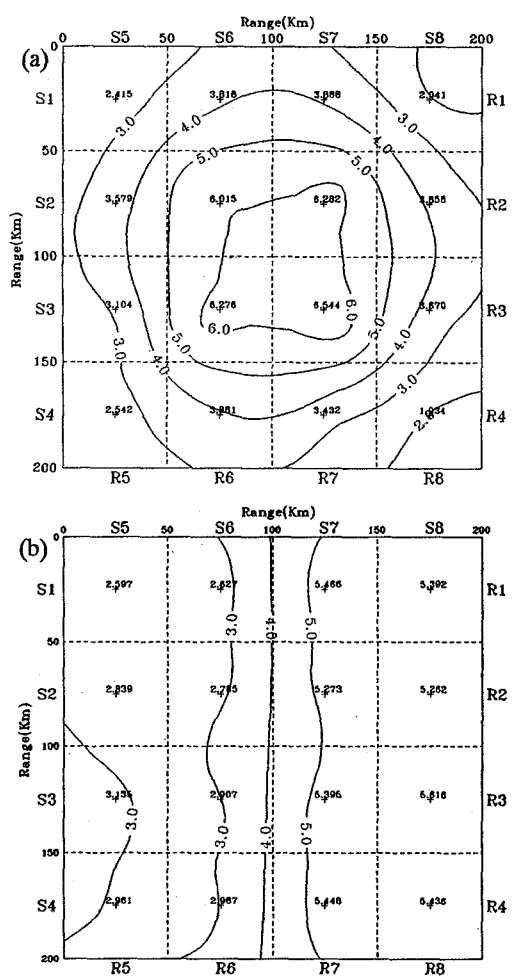

Fig. 8. Distribution of temperature estimated from the results of horizontal slice inversion for (a) the warm eddy and (b) the front at 200 m depth. The units is °C.

Table 2. Difference between the input temperatures and those based on inversion results at 400 m depth. (a) warm eddy where rms error is 0.372°C, (b) front where rms error is 0.337°C.

0.026	0.383	0.578	-0.132	0.390	0.074	-0.471	-0.440
0.520	-0.495	-0.269	0.402	0.464	0.037	-0.436	-0.618
0.295	-0.547	-0.396	0.506	-0.117	0.713	0.036	-0.193
0.037	0.652	0.616	0.090	-0.309	0.172	-0.537	-0.378

Table 3. Difference between the input temperatures and those based on inversion results at 200 m depth. (a) warm eddy where rms error is 1.059°C, (b) front where rms error is 1.672°C.

-1.492	-0.182	0.167	-1.755	0.371	0.688	0.127	-0.075
-0.291	-2.398	-2.020	-0.051	-1.991	-1.606	-1.238	-1.186
-0.790	-2.117	-1.563	-0.419	-1.217	-1.282	-3.072	-2.984
-1.271	-0.139	-0.364	-1.920	-3.880	-3.720	-1.654	-1.666

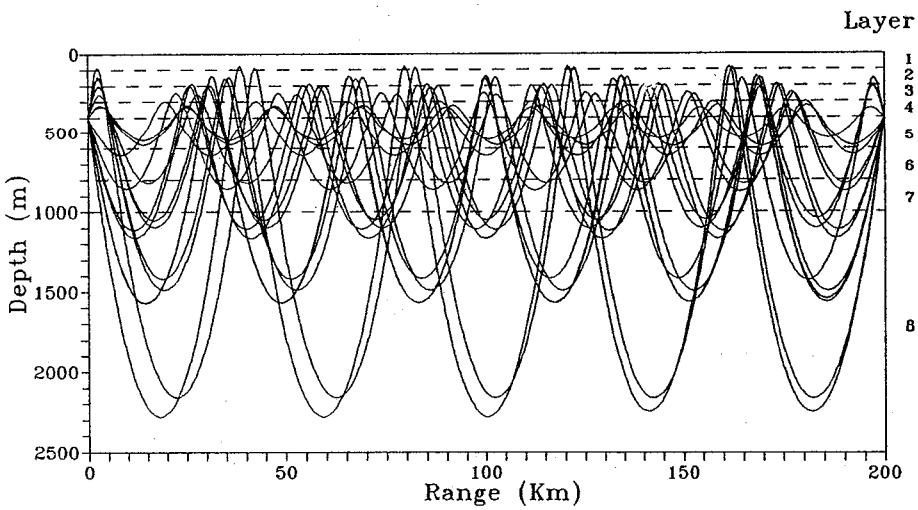

Fig. 9. Vertical slice gridding and eigenray paths for the canonical ocean.

3.0°C. It is believed that the error is mainly due to oscillation of ray path between the depth of 200 m and 1400 m. The acoustic travel times used in inversion rather represent the variations of temperature between 200 m and 1400 m depths than temperature distribution at 200 m depth. To reduce such an effect we corrected the inversion results at 200 m depth by using following empirical formula

$$C_{200} = (3\overline{C} - C_{400})/2, \quad (10)$$

where C_{200}: sound speed at 200 m

C_{400}: sound speed at 400 m

$\overline{C}$: average sound speed between 200~1400 m

C_{400} is the initial inversion results at 400 m depth and $\overline{C}$ is the average sound speed inversely estimated between 200 m and 1400 m depths. In equation (10), to obtain the sound speed at 200 m depth, we have considered the upper and lower turning depths which correspond to 200 m and 1400 m depths, respectively, and it gives the sound speed at 200 m depth as almost equal to the one at 1400 m depth (see Fig. 1).

Fig. 8 displays the final results of temperature distributions at 200 m depth. The results are improved compared to those of the first estimations and 400 m depth inversion. For the case of eddy input, the calculated temperatures are lower than those of the input data with rms error of about 1.0°C which is still bigger than errors at 400 m depth (Table 3a). A frontal structure (Fig. 8b) is also obtained but the temperature gradient is much stronger than that of input temperature in Fig. 4b. The rms error is about 1.7°C and the maximum error is about 3.9°C at the lower left cell (Table 3b).

Vertical Slice Inversion

To test the vertical slice tomography, the water column is divided into 8 layers as shown in Fig. 9: every 100 m from surface to 400 m depth, every 200 m from 400 m to 1000 m depth and 1 layer from 1000 m depth to the bottom (2500 m). The number of unknown values is 8 and more eigenray informations are needed to make the system overdetermined. The reference path lengths on each layer in the canonical ocean are presented in Table 4. It is assumed that a

Table 4. Path lengths R_{ij} (km) traveled by i th ray in j th layer on the vertical slice for the canonical ocean. Depth boundaries for each layer are given in the top row. Upper and lower turning depths for each ray given to left.

ray no. (i)	turning depth (km)		layer no. (j)							
			1	2	3	4	5	6	7	8
	upper	lower	0	0.1	0.2	0.3	0.4	0.6	0.8	1.0	2.5 km
1	0.077	2.275	2.10	9.17	9.17	9.17	18.34	18.34	18.34	116.87
2	0.086	2.159	1.43	10.21	10.21	10.21	20.42	20.42	20.42	118.31
3	0.093	2.063	0.72	10.22	10.22	10.22	20.44	20.44	20.44	108.66
4	0.139	1.567	0.0	8.58	14.07	14.07	28.14	28.14	28.14	79.76
5	0.141	1.544	0.0	7.75	13.13	13.13	26.26	26.26	26.26	71.44
6	0.139	1.566	0.0	8.59	14.08	14.08	28.16	28.16	28.16	79.71
7	0.157	1.405	0.0	6.92	16.09	16.09	32.18	32.18	32.18	65.16
8	0.189	1.160	0.0	2.27	20.65	20.65	41.30	41.30	41.30	33.05
9	0.200	1.095	0.0	0.0	22.40	22.40	44.80	44.80	44.80	21.28
10	0.194	1.131	0.0	1.28	21.41	21.41	42.82	42.82	42.82	28.04
11	0.206	1.058	0.0	0.0	22.12	23.53	47.06	47.06	47.06	13.65
12	0.247	0.847	0.0	0.0	17.69	33.38	66.76	66.76	15.69	0.0
13	0.258	0.795	0.0	0.0	15.66	37.29	74.58	72.71	0.0	0.0
14	0.247	0.847	0.0	0.0	17.69	33.38	66.76	66.76	15.69	0.0
15	0.293	0.665	0.0	0.0	3.77	53.80	107.60	34.97	0.0	0.0
16	0.327	0.566	0.0	0.0	0.0	61.11	138.96	0.0	0.0	0.0
17	0.328	0.563	0.0	0.0	0.0	61.30	138.77	0.0	0.0	0.0

ray path is straight between upper and lower turning points. The temperatures at each layer in vertical slice are computed by averaging the temperature perturbation from the reference value in the canonical ocean. The results display the range averaged vertical temperature (sound speed) profile not the profile in each cell as in horizontal slice inversion.

Results of the vertical slice inversion are presented as bold dashed line and the thin lines represent the temperature perturbation ($\delta\tau_i$) in Fig. 10. For the case of the eddy (Fig. 10a), temperature reconstructed by inversion is higher than the input temperature in the upper layers above 200 m depth. The vertical temperature gradient in the thermocline is larger than the input value. The mean of the errors is less than 1.0°C. For the frontal structure (Fig. 10b), the temperature from inversion are lower than the input data over the whole layer and the mean of the error is about 0.5°C. It is believed that most of the errors are due to the proportional ratio error of the the path length.

SUMMARY AND DISCUSSIONS

To develope ocean acoustic survey technology by using OAT in the East Sea, the canonical ocean of the study area has been established from long-term observations of temperature and salinity and the reference acoustic travel times and path lengths are calculated by using the acoustic model as a part of the forward model. The perturbed ocean structures are simulated by putting a mesoscale warm eddy and a thermal front into the canonical ocean. The experimental area is divided into 16 cells with 8 pairs of sources and receivers and the water column is divided into 8 layers to formulate an inverse problem. In this study, we have placed the sources and receivers at the mid point of the outer cells in order to increase the number of rank in SVD problem and to resolve the eddy or the frontal structure of 50×50 km scale. The estimated temperature field of horizontal slice at 400 m depth derived from the inverse method reflects the perturbed input of the warm eddy and the thermal front satisfactorily. The rms error of the horizontal slice is less than 0.4°C and 1.7°C at 400 m and 200 m depths, respectively. For vertical slice the rms error is less than 1.0°C while the tomographic temperatures are lower than the input values.

In the forward problem, the calculation of the initial or unperturbed travel time for each ray between the sources and receivers has been carried out using a range-independent ray model. In particular, the length of ray path in each vertical layer has been calculated by assuming the path to be a straight line between upper and lower turning points, thereby,

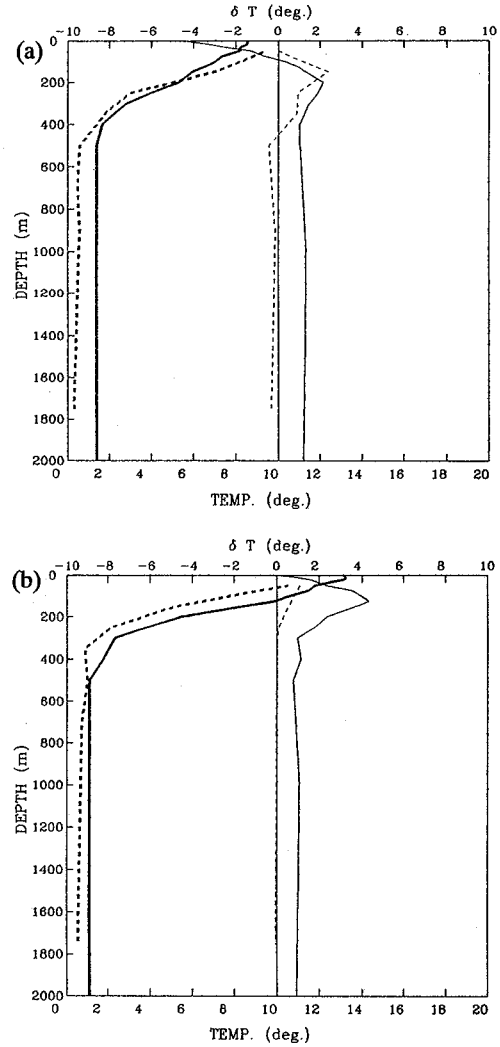

Fig. 10. Vertical slice of temperature (thick line) and temperature perturbation (thin line) obtained from the results of vertical slice inversion for (a) the warm eddy and (b) the front. Solid and dashed lines correspond to the input and inverse temperature and temperature perturbation.

neglecting any refraction effects within the layer. This may have produced errors in the travel time estimation. In order to reduce the error in both the horizontal and vertical slice, increment of number of sources and receivers may be possible, provided that the cost of handling is not a problem, but it is not a plausible solution. Rather, if a range-dependent ray model is used for inhomogeneous canonical ocean, more accurate ray travel times can be acquired. Also, a very significant source of error in vertical slice is due to the assumption of straight ray path in each vertical layer. Therefore, a new method to correctly estimate travel distance along any refracted ray should be developed for a reliable tomography experiment.

In conclusion, present experiment has been successful to predict, within permissible error range, the anomalous distribution of water temperature both in horizontal plane and in vertical plane. Further refinement in forward and inverse problem which has been indicated in the discussion is needed for future application of tomography to the real ocean survey.

ACKNOWLEDGEMENTS

This study was supported by grants given to the second author(J. Y., Na) KOSEF during 1993-1996 (93-0700-04-01-3). The third author(J. H., Lee) also acknowledge partial support of the Basic Research Program of Korea Ocean Research and Development Institute during 1995-1996. Careful readings and comments from reviewers are gratefully acknowledged.

REFERENCES

Aki, K. and P.G. Richards, 1980, *Qualitative Seismology: Theory and methods*, W. H. Freeman and Company, New York, 923 pp.

Akulichev, V.A. and A.A Solovyov, 1993, Acoustic thermometry in the North Pacific Ocean in the Sea of Japan, 2nd Int. Meeting of Global Acoustic Monitoring in the Ocean, June 20-22, Brest, France.

Bennett, A.F., 1992, *Inverse Methods in Physical Oceanography*, Cambridge University Press, New York, 346 pp.

Clay, C.S. and H. Medwin, 1977, *Acoustical Oceanography: Principles and Applications*, Jhon Wiley & Sons, Inc., New York, 544 pp.

Cornuelle, B.D., C. Wunsch, D. Behringer, T.G. Birdsall, M. Brown, R. Heinmiller, R.A. Knox, K. Metzger, W.H. Munk, J.L. Spiesberger. R.C. Spindel, D. Webb and P.E. Worcestor, 1985, Tomographic maps of the ocean mesoscale, 1: Pure acoustics, *J. Phys. Oceanogr.*, **15**: 133-152.

FRDA, 1986, Mean Oceanographic Charts of the Adjacent Seas of Korea, Fisheries Research and Development Agency, Pusan, 186 pp.

Han, S.K., and J.Y. Na, 1994, Feasibility of ocean survey by using ocean acoustic tomography in the sou-

thwestern part of the East Sea, *J. Acoust. Soc. Kor.*, **13**(6): 75-82.

Howe, B.M., P.F. Worcester and R.C. Spindel, 1987, Ocean acoustic tomography: Mesoscale velocity, *J. Geophys. Res.*, **92**(C4): 3785-3805.

Kaneko, A., G. Yuan, N. Gohda and I. Nakano, 1994, Optimum design of the ocean acoustic tomography system for the Sea of Japan, *J. Oceanogr.*, **50**: 281-293.

Lanczos, C., 1961, *Linear Differential Operators*, Van Nostrand, New York.

Lawrence, W., and J.L. Spiesberger, 1989, Measurements of a barotropic planetary vorticity mode in an eddy-resolving quasi-geostrophic model using acoustic tomography, *J. Phys. Oceanogr.*, **19**: 865-873.

Lynch, J., D. Frye, K. Peal, S. Liberatore, S. Kery, E. Hobart, A Newhall and S. Smith, 1992, Real-time tomography mooring, WHOI Technical Report, WHOI-92-29.

Lynch, J.F., G. Jin, R. Pawlowicz, D. Ray, C.-S. Chiu, J. H. Miller, R.H. Bourke, A.R. Parsons and R. Muench, 1996, Acoustic travel-time perturbations due to shallow-water internal waves and internal tides in the Barents Sea Polar Front: Theory and experiment, *J. Acoust. Soc. Am.*, **99**(2): 803-821.

Munk, W.M. and A.M.G. Forbes, 1989, Global ocean warming: An acoustic measure ?, *J. Phys. Oceanogr.*, **19**: 1765-1778.

Munk, W., P. Worcestor and C. Wunsch, 1995, Ocean acoustic tomography, Cambridge University Press, New York, 433 pp.

Munk, W.M. and C.A. Wunsch, 1979, Ocean acoustic tomography: A scheme for large scale monitoring, *Deep-Sea Res.*, **26**: 123-161.

Na, J.-Y., and S.-K. Han, 1994, Simulation of underwater signal in the East Sea of Korea for application of ocean acoustic tomography, *WESTPRAC V*, 23-25, Aug., Seoul, 401-408.

Paeng, D.K., 1993, Acoustic characteristics of the eddies in the East Sea of Korea, MS Thesis, Hanyang University, 80 pp.

Spiesberger, J.L., R.C. Spindel and K. Metzger, 1980, Stability and identification of ocean acoustic multipaths, *J. Acoust. Soc. Am.*, **67**: 2011-2017.

Worcester, P.F., B.D. Cornuelle and R.C. Spindel, 1991, A review of ocean acoustic tomography : 1987-1990, *Rev. Geophys., Supplement*: 557-570.